




Scaling of the ^{19}B two-neutron halo properties close to unitarityEmiko Hiyama,^{1,2} Rimantas Lazauskas³,,³ Jaume Carbonell⁴,,⁴ and Tobias Frederico⁵¹*Department of Physics, Tohoku University, Sendai 980-8578, Japan*²*RIKEN, Nishina Center, Wako, Saitama 351-0198, Japan*³*Université de Strasbourg, CNRS, IPHC UMR 7178, F-67000 Strasbourg, France*⁴*Université Paris-Saclay, CNRS/IN2P3, IJCLab, F-91405 Orsay, France*⁵*Instituto Tecnológico de Aeronáutica, 12.228-900 São José dos Campos, Brazil*

(Received 24 August 2022; accepted 17 November 2022; published 1 December 2022)

We explore the description of the bound ^{19}B isotope in terms of a $^{17}\text{B} + n + n$ three-body system where the two-body subsystems $^{17}\text{B} + n$ and neutron-neutron (nn) have virtual states close to the continuum. Dimensionless scaling functions for the root-mean-square (rms) radii are defined and studied for different parameters of the neutron-core potential and considering three different models for neutron-neutron interaction. The scaling functions for the radii are rooted in the universal behavior of three-body systems close to the Efimov limit and depend only on dimensionless quantities formed by the two-neutron separation energies and scattering lengths. Our results show in practice the model independence of these scaling functions close to unitarity. We provide an estimation of the different rms relative separation distances between the constituents, as well as of the proton and matter radii.

DOI: [10.1103/PhysRevC.106.064001](https://doi.org/10.1103/PhysRevC.106.064001)

I. INTRODUCTION

Weakly bound light radioactive nuclei having the structure of a core $+ n + n$ are found in the vicinity of the neutron drip line and share the characteristic property of forming a large two-neutron halo [1]. The neutron halo is markedly situated outside the n -core interaction range, and it is governed by a large n -core s -wave scattering length, exceeding by far the effective range. Much has been discussed on the structure and reactions of light two-neutron halo nuclei close to the drip line since the pioneering work on ^{11}Li [2], with an extensive review literature [3–14]. To cite one example, it has been pointed out theoretically that ^{22}C has a $n - ^{20}\text{C}$ subsystem with a large s -wave scattering length, and then as a result the three-body system, namely $^{20}\text{C} - n - n$, forms a weakly bound Borromean state of ^{22}C [15–17], which is supported by analysis of earlier experiments [18] and by the more recent observation and analysis of higher-precision cross sections [19].

In 2010, the weakly bound Borromean state of ^{19}B [20] was observed. The paper reported that a virtual state of ^{18}B is located below the $^{17}\text{B} + n$ threshold and that the scattering length of $^{17}\text{B} + n$, a_S , was negative and large. However, due to the poor resolution and acceptance of the experiment, the precise value of the scattering length was not determined and only an upper bound $a_S < -50$ fm was established. The two-neutron separation energy, S_{2n} of ^{19}B was measured in another experiment [21], where it was reported to be 0.14 ± 0.39 MeV. A more recent compilation of nuclear masses provides $S_{2n} = 0.09 \pm 0.56$ MeV [22].

Motivated by these experiments, some of the present authors (E.H., R.L., and J.C.) studied the structure of ^{19}B within the framework of a $^{17}\text{B} + n + n$ three-body model [23] and

predicted the binding energy of the ground state in ^{19}B by tuning the $n - ^{17}\text{B}$ scattering length ($-100 < a_S < -20$ fm). The two-neutron separation energy value of $S_{2n} = 0.13$ MeV was found by considering $a_S = -100$ fm, which is compatible with the experimental data [21]. In addition, due to the large magnitude of the $^{17}\text{B} + n$ scattering length, it was pointed out that the ground state has features of an Efimov state [24,25]; however, due to the unfavorable heavy-light-light mass composition of this three-cluster state it is highly unlikely to form an Efimov excited state. That, indeed, is excluded by the possible regions of existence of such states systematized in Ref. [26] and later on within Effective Field Theory (EFT) in [27]. Despite that, the shallow ground state of the large two-neutron halo of ^{19}B should exhibit universal and model independent properties through its structure, which would be dominated by what is known as Efimov physics [28]: An intrinsic consequence of the discrete scale invariance in the unitarity limit, or equivalently in the zero-range interaction limit (see, e.g., [6]).

Furthermore, a new experiment on ^{19}B was recently performed [29]. An enhanced soft electric-dipole mode just above the two-neutron decay threshold was observed, and properly interpreted within three-body calculations that reproduce the energy spectrum. They found the best fit of the relative energy spectrum for $S_{2n} = 0.5$ MeV, $a_S = -50$ fm, resulting in a rms radius of the core with respect the two-neutron center of mass given by

$$\sqrt{\langle r_{c-2n}^2 \rangle} = 5.75 \pm 0.11 \text{ (stat)} \pm 0.21 \text{ (sys) fm}, \quad (1)$$

similar in size to the corresponding quantity in ^{11}Li . It was concluded that the valence neutrons have a significant s -wave configuration and exhibit a pronounced neutron-neutron correlation. Apart from the experimental activity, theoretical efforts were expended to study the structure of ^{19}B in a three-body model [30] and also within the many-body mean-field approach of the deformed relativistic Hartree-Bogoliubov theory in the continuum [31].

In present paper, we study the universal features of the structure of the shallow Efimov-like ^{19}B ground state from another perspective. We establish the appropriate ^{19}B scaling functions for the different rms radii close to the unitarity limit, which depend only on two-dimensionless quantities formed by the two-neutron separation energies and scattering lengths. That approach was proposed for general three-body systems interacting via s -wave zero-range potentials in Ref. [32]. Such scaling functions describe universal correlations between observables and they appear as limit cycles from the discrete scale symmetry that the system presents when the potential range is driven to zero or the scattering lengths to infinity [6], which can also be built within the context of EFT [27]. The limit cycles for the scaling functions associated with correlations between dimensionless quantities are built from successive Efimov or Thomas collapsed states.

These correlations between observables represent, modulo effective-range corrections, the results obtained from short-range potentials for shallow states. They should be quite model independent, which can be verified with the use of different potentials that share the same two-body low-energy s -wave observables. In light of the concepts of universal scaling functions and using the newly extracted $2n$ separation energy, a_S , and $\langle r_{c-2n}^2 \rangle^{\frac{1}{2}}$ for this system [29], we compute the ^{19}B matter and proton rms radii, and also the different rms relative separation distances. We check the consistence of these extracted data comparing results of different potential models for the n -core and nn systems, as well as calculations from other authors, to assert the model independence of the scaling laws. Therefore, we expect that this work can be also viewed as a useful model independent systematic to predict long wavelength observables on the basis of a minimal number of physical inputs.

The work is organized as follows. In Sec. II, we briefly review the model from Ref. [23] for the neutron-core interaction based on a parametrization of the MT13 potential. In Sec. III, we introduce the relevant scaling functions for the two-neutron separation energy and the different rms radii. Next, we present the calculation of the scaling function for S_{2n} , the radii vs a_S and S_{2n} , and perform the scaling analysis for the rms radii, aiming to demonstrate the model independence of this correlation. In Sec. IV our final remarks are presented; we show in addition some results for the matter and proton rms radius based on our analysis through the scaling functions.

II. MODELING ^{19}B

As proposed in Ref. [23], the ^{19}B isotope is described as a $^{17}\text{B} + n + n$ three-body system. To this aim, we first constructed an effective low-energy $n - ^{17}\text{B}$ potential, simulating

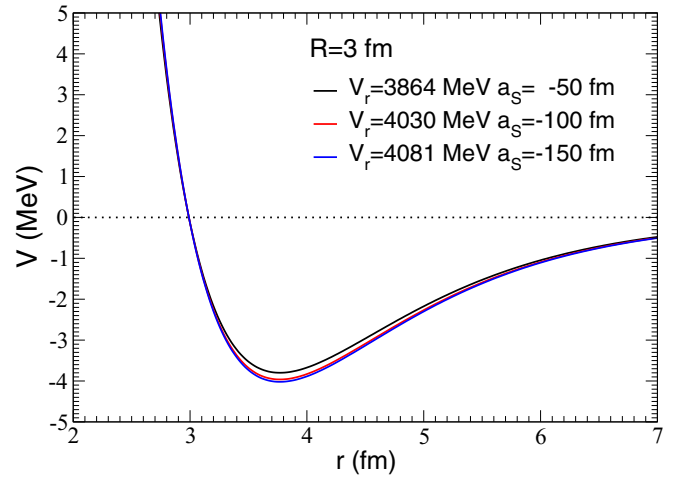


FIG. 1. $V_{n^{17}\text{B}}$ potential (MeV) reproducing several values of the $n - ^{17}\text{B}$ scattering length a_S (fm) and the corresponding strength parameters V_r

the short-range Pauli repulsion at distances smaller than the ^{17}B core radius, which is outweighed by the folded attractive nucleon-nucleon interaction beyond this overlap region. A simple form accounting for these facts is

$$V_{n^{17}\text{B}}(r) = V_r \frac{e^{-2\mu r}}{r} [1 - e^{-\mu(R-r)}], \quad (2)$$

where R is the hard-core radius and μ is a range parameter for the Yukawa $n - ^{17}\text{B}$ potential. We have chosen the value $R = 3$ fm, which corresponds to the rms matter radius of ^{17}B [33], and we take $\mu = 0.7\text{fm}^{-1}$ corresponding to the pion mass.

After fixing the range μ and the size R , potential (2) depends on a single strength parameter V_r , which is tuned to reproduce the $n - ^{17}\text{B}$ scattering length a_S . We display in Fig. 1 the potentials reproducing the values $a_S = -50, -100, -150$ fm with the corresponding strength parameters V_r (MeV).

All the numerical values along this work correspond to $m_n = 939.5654$ MeV, $m_{^{17}\text{B}} = 15879.1$ MeV, i.e., a $n - ^{17}\text{B}$ reduced mass $m_R = 887.0771$ MeV and $\hbar^2/2m_R = 21.9473$ MeV fm 2 .

The interaction (2) is purely central and independent of the total spin \vec{S} of the $n + ^{17}\text{B}$ system ($\vec{S} = \vec{s}_n + \vec{S}_{^{17}\text{B}}$). Since ^{17}B is a $J^\pi = 3/2^-$ state, it can couple to a neutron in two different total spin states, $S = 1^-, 2^-$. This “spin-symmetric” approximation could be not very realistic given that, according to [20], the $S = 2^-$ state has a resonant scattering length and there is no reason that the $S = 1^-$ would be resonant as well. Nevertheless, for the sake of simplicity we decided to stick with a spin-independent form of $n + ^{17}\text{B}$ interaction, whose strength is directly associated with a single unknown: $n + ^{17}\text{B}$ scattering length a_S .

The ^{19}B Hamiltonian requires also the nn interaction and we have used in our calculations three different V_{nn} models. We have considered the charge independent (CI) Bonn-A model [34] providing the nn low energy parameters $a_{nn} = -23.75$ fm and $r_{nn} = 2.77$ fm, and the charge dependent (CD) AV18 [35] for which $a_{nn} = -18.8$ fm and $r_{nn} = 2.83$ fm, both

TABLE I. Dependence on the singlet $n + ^{17}\text{B}$ scattering length of the two-neutron separation energy and rms relative separation distances in the $^{17}\text{B} + n + n$ system computed with the Bonn-A and MT13 nn potentials for $R = 3$ fm. S_{2n} are in MeV, a_S and $\langle r_\alpha^2 \rangle^{\frac{1}{2}}$ are in fm ($\alpha = nn, c - 2n, nc$).

a_S	S_{2n}	$\langle r_{nn}^2 \rangle^{\frac{1}{2}}$	$\langle r_{c-2n}^2 \rangle^{\frac{1}{2}}$	$\langle r_{nc}^2 \rangle^{\frac{1}{2}}$
Bonn-A				
-50	0.087031	16.15	10.89	13.56
-80	0.117391	14.79	10.11	12.53
-100	0.128790	14.40	9.89	12.23
-300	0.162571	13.45	9.35	11.52
-500	0.169934	13.28	9.25	11.39
-1000	0.175789	13.15	9.18	11.29
MT13				
-50	0.063234	18.24	11.78	14.90
-80	0.090628	16.43	10.77	13.55
-100	0.101013	15.92	10.49	13.17
-300	0.132020	14.72	9.82	12.27
-500	0.138816	14.51	9.70	12.11
-1000	0.144228	14.35	9.61	11.99

models acting in all partial waves. We have also considered the S -wave CD version of MT13 [36] built in [23] with low-energy parameters $a_{nn} = -18.59$ fm and $r_{nn} = 2.93$ fm, in agreement with the experimental values. It takes the form

$$V_{nn} = V_R \frac{e^{-\mu_R r}}{r} - V_A \frac{e^{-\mu_A r}}{r}, \quad (3)$$

where the parameters are $V_R = 1438.720$ MeV fm, $V_A = 509.40$ MeV fm, $\mu_R^{-1} = 3.11$ fm, $\mu_A^{-1} = 1.55$ fm.

III. ^{19}B RESULTS

We have computed the ^{19}B ground-state energy, measured by the two-neutron separation energy S_{2n} as a function of a_S . The rms relative separation distances were also calculated for $\langle r_{nn}^2 \rangle^{\frac{1}{2}}$, $\langle r_{nc}^2 \rangle^{\frac{1}{2}}$, $\langle r_{c-2n}^2 \rangle^{\frac{1}{2}}$, $\langle r_n^2 \rangle^{\frac{1}{2}}$, and $\langle r_c^2 \rangle^{\frac{1}{2}}$. The three-body problem was solved by the Gaussian expansion method [37] and by the Faddeev equation formalism in configuration space [38,39].

In Table I, we present an example of our results obtained with both Bonn-A and MT13 potentials, where the dependence on the spin independent $n + ^{17}\text{B}$ scattering length is explored for the two-neutron separation energy and different rms relative separation distances in the Borromean $^{17}\text{B} + n + n$ system. As it should, S_{2n} increases towards unitarity as $V_{n^{17}\text{B}}$ becomes slightly more attractive, despite the two neutron separation energy remains below 0.2 MeV, implying in a giant halo around 10 fm, to be compared with the smaller size of the core nucleus. Such values of S_{2n} are consistent with $S_{2n} = 0.14 \pm 0.39$ MeV [21].

Furthermore, by using the results presented in Table I the neutron and core rms distances to the center of mass can be easily evaluated from $\langle r_{nn}^2 \rangle^{\frac{1}{2}}$, $\langle r_{c-2n}^2 \rangle^{\frac{1}{2}}$, and $\langle r_{nc}^2 \rangle^{\frac{1}{2}}$, given

respectively by

$$\langle r_n^2 \rangle^{\frac{1}{2}} = \sqrt{\frac{2A \langle r_{nc}^2 \rangle + \langle r_{nn}^2 \rangle}{2(A+2)} - \frac{2A \langle r_{c-2n}^2 \rangle}{(A+2)^2}}, \quad (4)$$

and $\langle r_c^2 \rangle^{\frac{1}{2}} = 2 \langle r_{c-2n}^2 \rangle^{\frac{1}{2}} / (A+2)$, with A the ^{17}B mass number. Also, the average relative angles, which are given by

$$\theta_{nc} = \cos^{-1} \frac{\langle \vec{r}_c \cdot \vec{r}_n \rangle}{\sqrt{\langle r_c^2 \rangle \langle r_n^2 \rangle}} = \cos^{-1} \frac{\langle r_c^2 \rangle + \langle r_n^2 \rangle - \langle r_{nc}^2 \rangle}{2\sqrt{\langle r_c^2 \rangle \langle r_n^2 \rangle}},$$

$$\theta_{nn'} = \cos^{-1} \frac{\langle \vec{r}_n \cdot \vec{r}_{n'} \rangle}{\langle r_n^2 \rangle} = \cos^{-1} \left(1 - \frac{1}{2} \frac{\langle r_{nn}^2 \rangle}{\langle r_n^2 \rangle} \right), \quad (5)$$

quantify the geometry of the halo and verify

$$\theta_{nn'} + 2\theta_{nc} = 360^\circ,$$

that is accurately fulfilled in our calculations.

A. Scaling functions

Within the considered model, the $^{17}\text{B} + n + n$ system is loosely bound, such that its giant halo has rms relative distances one order of magnitude larger than the interaction range ≈ 1 fm. One should notice, however, that the nn effective ranges are only about four times smaller than these sizes, thus indicating a possible relevance of the range corrections. Under this condition we will study the results of Table I systematically employing the halo universal scaling laws (see, e.g., [6]), emerging as a consequence of the correlations between observables of Efimov-like states.

Close to the unitarity limit, these scaling laws depend only on the scattering lengths, the two neutron separation energy, and core mass number. The energy scaling function as introduced in [40] is the correlation between the three-body energy at a given scattering length with the value at the unitarity. The range dependence was also taken into account, which we will not display here:

$$\frac{S_{2n}}{S_{2n}^{un}} = \mathcal{F}([a_S \kappa_{nc}]^{-1}, [a_{nn} \kappa_{nn}]^{-1}, A), \quad (6)$$

where

$$\kappa_{nc} = (2\mu_{nc} S_{2n})^{\frac{1}{2}}, \quad \kappa_{nn} = (m_n S_{2n})^{\frac{1}{2}}, \quad (7)$$

and μ_{nc} is the reduced mass of the n -core system and S_{2n}^{un} is the two-neutron separation energy at unitarity. The last scaling relation is written by considering $\hbar = m_n = 1$ and it attains the trivial value 1 at unitarity.

Other scaling functions can be found for the rms relative separation distances, and they read [32] (see also [6] for further discussions)

$$\langle r_\alpha^2 \rangle \sqrt{S_{2n}} = \mathcal{R}_\alpha([a_S \kappa_{nc}]^{-1}, [a_{nn} \kappa_{nn}]^{-1}, A), \quad (8)$$

where α denotes the possible relative distances: nn (neutron-neutron), nc (neutron-core), $c-2n$ (core- nn c.m.), n (neutron-c.m.) and c (^{17}B -c.m.). The angles defined by Eq. (5) are a consequence of Eq. (8) scaling functions determined, in principle, by the limit cycles of the different radii.

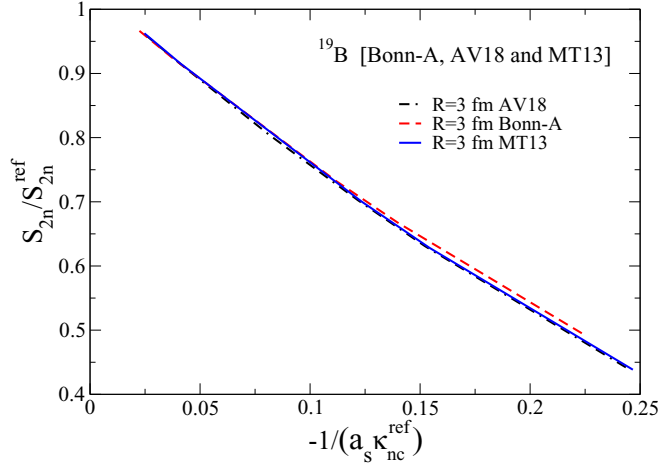


FIG. 2. Ratio between the two-neutron separation energy (S_{2n}) of ^{19}B and a reference one (S_{2n}^{ref}) as function of $-1/(2\mu_{nc}a_s^2 S_{2n}^{\text{ref}})^{1/2}$. The results are obtained with $R = 3$ fm for the Bonn-A (dashed line), MT13 (solid line), and AV18 (dot-dashed line) nn potentials. The reference two-neutron separation energy is explained in the text.

The unitarity limit of the scaling relations are found for $1/(a_s \kappa_{nc}) = 1/(a_{nn} \kappa_{nn}) = 0$ as

$$\langle r_\alpha^2 \rangle_{un} \sqrt{S_{2n}^{un}} = \mathcal{R}_\alpha(0, 0, A), \quad (9)$$

which was discussed in [6], and are only a function of the core mass number. Another universal property of the scaling function (8) is [6]

$$\frac{\partial}{\partial z_i} \mathcal{R}_\alpha(z_1, z_2, A) > 0, \quad (10)$$

which means, in particular, that the halo system shrinks when it moves from unitarity to a Borromean configuration. This is natural as the system has to compress in order to preserve the same binding energy when it is driven from unitarity to a Borromean state [32]. Indeed, such behavior is also confirmed in present calculations, as we will illustrate in what follows.

B. Scaling analysis for S_{2n}

The scaling function of the two-neutron separation energy for the Borromean system ^{19}B is shown in Fig. 2 in terms of a reference value:

$$\frac{S_{2n}}{S_{2n}^{\text{ref}}} = \mathcal{F}([a_s \kappa_{nc}^{\text{ref}}]^{-1}, [a_{nn} \kappa_{nn}^{\text{ref}}]^{-1}, A), \quad (11)$$

with the definitions

$$\kappa_{nc}^{\text{ref}} = (2\mu_{nc} S_{2n}^{\text{ref}})^{1/2} \quad \text{and} \quad \kappa_{nn}^{\text{ref}} = (m_n S_{2n}^{\text{ref}})^{1/2}. \quad (12)$$

We make use of the general form provided by Eq. (6), with the arguments corresponding to $a_s = -1000$ fm for $S_{2n}^{\text{ref}} = 0.1758$ MeV and $S_{2n}^{\text{ref}} = 0.1442$ MeV, as given in Table I for AV18, Bonn-A, and MT13 nn potentials, respectively. For the AV18 interaction we have $S_{2n}^{\text{ref}} = 0.1481$ MeV for $R = 3$ fm and $a_s = -1000$ fm.

We observe that the slope is weakly dependent on the nn interaction model, confirming the validity of an universal

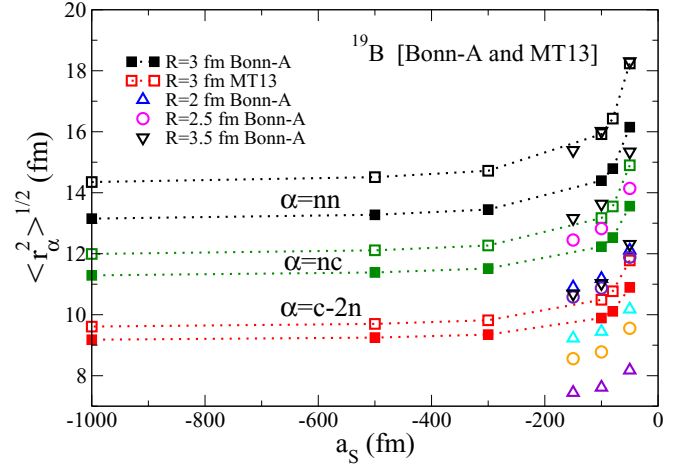


FIG. 3. ^{19}B rms radii ($\langle r_\alpha^2 \rangle^{1/2}$ ($\alpha \equiv nn, nc, c - 2n$)) as a function of the scattering length a_s . Full squares are the results for Bonn-A and empty squares for MT13 nn potentials, all of them with $R = 3$ fm. Empty triangles and circles correspond to Bonn-A with other choices of R : Down-triangles with $R = 3.5$ fm, up-triangles with $R = 2$ fm, empty circles with $R = 2.5$ fm. Dotted lines connecting the results are for guidance.

scaling law. The curves in the figure can be parameterized by

$$\begin{aligned} \left. \frac{S_{2n}}{S_{2n}^{\text{ref}}} \right|_{\text{Bonn-A}} &= 1.03 - \frac{2.94}{a_s \kappa_{nc}^{\text{ref}}} + \frac{2.43}{(a_s \kappa_{nc}^{\text{ref}})^2} + \dots, \\ \left. \frac{S_{2n}}{S_{2n}^{\text{ref}}} \right|_{\text{MT13}} &= 1.04 - \frac{3.00}{a_s \kappa_{nc}^{\text{ref}}} + \frac{2.38}{(a_s \kappa_{nc}^{\text{ref}})^2} + \dots, \\ \left. \frac{S_{2n}}{S_{2n}^{\text{ref}}} \right|_{\text{AV18}} &= 1.04 - \frac{3.02}{a_s \kappa_{nc}^{\text{ref}}} + \frac{2.42}{(a_s \kappa_{nc}^{\text{ref}})^2} + \dots, \end{aligned} \quad (13)$$

which also shows that the difference between the nn scattering lengths and effective ranges of Bonn-A and MT13 is not significant for this particular scaling function. The 3–4% deviation from unity at $1/a_s = 0$ in Eq. (13) shows that the reference S_{2n}^{ref} values are indeed quite close to this situation. As a reference the linear coefficients, associated with Tan's contact [41], are close to 3 in the three cases, which could be compared to 2.11 [40,42,43] for the three-boson system. The quadratic coefficients are about 2.4 compared to 0.80 in the three-boson case [40]. We observe that this correlation is quite insensitive to the different values of a_{nn} in the three potential models for a fixed R . Furthermore, as the system shifts from the unitarity to Borromean, the separation energy tends to decrease with respect to the unitarity value, since the interaction becomes weaker.

C. Radii versus a_s and S_{2n}

The ^{19}B rms radii ($\langle r_\alpha^2 \rangle^{1/2}$ ($\alpha \equiv nn, nc, c-2n$)) as a function of a_s are displayed in Fig. 3, for the calculations with $R = 3$ fm, given in Table I, and also for R assuming the values of 2, 2.5 and 3.5 fm in the case of the Bonn-A potential. The rms radii for the Bonn-A potential are systematically smaller

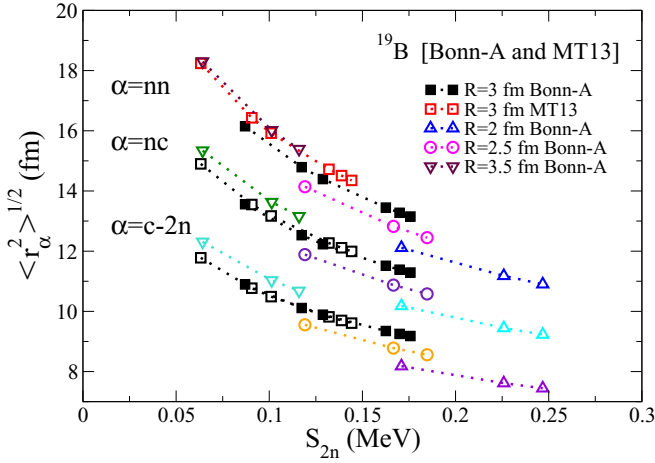


FIG. 4. ^{19}B root mean square radii $\langle r_\alpha^2 \rangle^{1/2}$ ($\alpha \equiv nn, nc, c-2n$) as a function of the two-neutron separation energy. Symbols and lines are the same as in Fig. 3.

than the ones for MT13. The size of ^{19}B increases when the scattering lengths decrease, for the dependence in both a_S and a_{nn} .

At first sight, it seems to be in conflict with the monotonic behavior found for the rms radii scaling functions expressed by Eq. (10). However, we must remind the reader that also the correlation with S_{2n} is relevant for these ^{19}B quantities, as the three-body system in this lowest angular momentum state is sensitive to the short range physics determining the actual values of the separation energies. This feature is revealed in Fig. 4, where the results for the different radii from Table I demonstrate a strong correlation with the two-neutron separation energy. However, the values of the dimensionless products $1/(a_S \kappa_{nc})$ and $1/(a_{nn} \kappa_{nn})$ move along these curves, as well as the different values of the core radius potential parameter R , which takes the values 2, 2.5, 3 and 3.5 fm, making the results somewhat scattered in the figure.

In order to organize these results, it is convenient to study the radii scaling laws for the three-body system in more detail.

D. Scaling analysis for the rms radii

Our task now is to provide the scaling analysis of the dimensionless products $\langle (r_\alpha^2) S_{2n} \rangle^{1/2}$ ($\alpha \equiv nn, nc, c-2n$), neutron-c.m. ($\alpha = n$) and core-c.m. ($\alpha = c$) as a function of $-1/(a_S \kappa_{nc})$ for the three employed neutron-neutron potentials: Bonn-A, AV18, and MT13. In the present analysis the scaling functions, as formulated in Eq. (8), are plotted, in what follows, against $1/(a_S \kappa_{nc})$. Here one should notice that the products $1/(a_{nn} \kappa_{nn})$ are implicitly running with S_{2n} .

In Fig. 5 the dimensionless products $\langle (r_\alpha^2) S_{2n} \rangle^{1/2}$ ($\alpha \equiv nn, nc, c-2n$) as a function of $-1/(a_S \kappa_{nc})$, for Bonn-A, AV18, and MT13 potentials are presented. The zero-range limit at unitarity $\langle (r_{nn}^2) S_{2n} \rangle^{1/2}|_{zr} = 0.8$ and $\langle (r_{nc}^2) S_{2n} \rangle^{1/2}|_{zr} = 0.7$ (see [6] and references therein) are reasonably close to the present calculations when $1/(a_S \kappa_{nc})$ approaches zero. It is worth noticing that both the neutron-neutron scattering lengths as well as effective ranges are finite, which of course differs from the

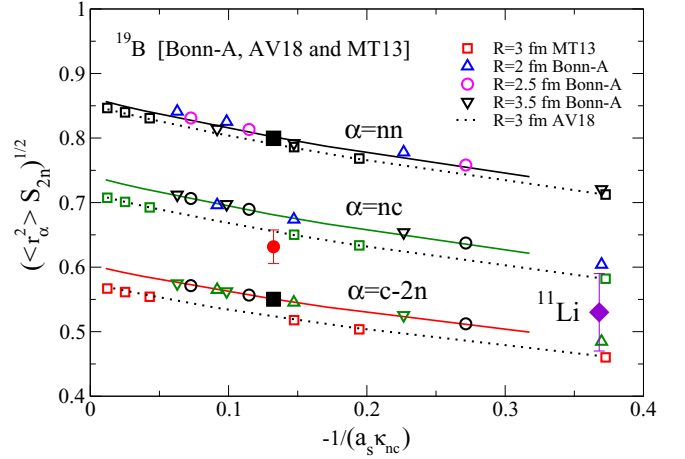


FIG. 5. ^{19}B dimensionless products $\langle (r_\alpha^2) S_{2n} \rangle^{1/2}$ ($\alpha \equiv nn, nc, c-2n$) as a function of $-1/(a_S \kappa_{nc})$, where $\kappa_{nc} = (2\mu_{nc} S_{2n})^{1/2}$. Results corresponding to $R = 3$ fm are indicated by solid lines for Bonn-A, by empty squares for MT13, and by dotted lines for AV18 nn potentials. Those with $R = 2, 2.5, 3.5$ fm obtained with the Bonn-A potential are denoted by up-triangle, empty circle, and down-triangle, respectively. Full squares correspond to the three-body calculations of Ref. [30]. The full circle is the experimental extraction of Ref. [29]. The full diamond is the estimated value of $\langle ({}^{11}\text{Li} | r_{c-2n}^2 | {}^{11}\text{Li} \rangle S_{2n}^{11}\text{Li})^{1/2}$ (see text for explanation).

strict unitarity limit, defined by infinite scattering lengths and vanishing effective ranges.

The effect of the a_{nn} , being slightly different for Bonn-A and MT13 or AV18, might be noticed in the figure, with the MT13 and AV18 results systematically lower than the Bonn-A ones. On the other hand, a_{nn} for AV18 and MT13 differ only by 1% and this difference is not enough to make an observable shift in the figure. The somewhat lower values obtained for MT13 and AV18 with respect to Bonn-A are due to

$$1/(a_{nn} \kappa_{nn})^{1/2}|_{\text{MT13}} < 1/(a_{nn} \kappa_{nn})^{1/2}|_{\text{Bonn-A}},$$

which makes the two-neutron halo of ^{19}B more compact for the MT13 model, consistent with the monotonically increasing behavior expressed by the partial derivatives given in Eq. (10) for the radii scaling functions.

We compare the scaling functions in Fig. 5 with the calculation from [30]. The last calculations employed a Woods-Saxon (WS) plus spin-orbit neutron- ^{17}B potential, the Gogny-Pires-Tourreil (GPT) neutron-neutron one [44] ($a_{nn} = -22.12$ fm and $r_{nn} = 2.83$ fm) in conjunction with hyperradial Gaussian three-body potential tuned to fit $S_{2n} = 0.5$ MeV. The central part of the WS potential gives $a_S = -50$ fm, and the strength of the spin-orbit term is determined to fit the position of a $d_{5/2}$ resonance at 1.1 MeV above the ^{17}B -neutron continuum close to the 1^- state from shell-model calculations [20]. Their results are $\langle r_{nn}^2 \rangle^{1/2} = 7.28$ fm and $\langle r_{c-2n}^2 \rangle^{1/2} = 5.01$ fm, giving respectively $\sqrt{\langle r_{nn}^2 \rangle S_{2n}} = 0.80$ and $\sqrt{\langle r_{c-2n}^2 \rangle S_{2n}} = 0.55$, consistent with our results for Bonn-A potential, which has effective range by 10% smaller. The fine tuning of the

calculations requires all low-energy parameters to be identical. Despite of that the comparison shows the extend of model dependence that the scaling functions may have.

The data with error bars in Fig. 5 were obtained from the radius extraction performed in [29], where ^{19}B has been studied by exclusive measurements of $^{17}\text{B} + n + n$ from the Coulomb breakup reaction with Pb at 220 MeV/nucleon. Three-body calculations were used to reproduce the soft $E1$ energy excitation spectrum below 6 MeV, and indicated that the valence neutrons have a significant dineutron correlation in an s -wave configuration. Furthermore, the $^{17}\text{B} + n + n$ three-body model calculations performed to analyze the experimental results using $a_S = -50$ fm and $S_{2n} = 0.5$ MeV extracted the value for $\langle r_{c-2n}^2 \rangle^{1/2}$ written in (1), which gives $(\langle r_{c-2n}^2 \rangle S_{2n})^{1/2} = 0.632 \pm 0.026$ for $1/(a_S \kappa_{nc}) = -0.1325$.

We also compared the results for the scaling function given in Fig. 5 to the estimated ^{11}Li core- $2n$ distance, which is found within the interval 5.01 ± 0.32 [45] to 6.2 ± 0.5 fm [7], corresponding to

$$0.47 \lesssim (\langle ^{11}\text{Li} | r_{c-2n}^2 | ^{11}\text{Li} \rangle S_{2n}^{11\text{Li}})^{1/2} \lesssim 0.59,$$

using the experimental value $S_{2n}^{11\text{Li}} = 369.15(65)$ keV [46]. This last value gives $1/(a_{n-9\text{Li}} \kappa_{nc}) = -0.368$ considering the s -wave virtual state of ^{10}Li to be at -50 keV.

The upper panel of Fig. 6 shows the ^{19}B dimensionless products $(\langle r_\alpha^2 \rangle S_{2n})^{1/2}$ ($\alpha \equiv n, c$) as a function of $-1/(a_S \kappa_{nc})$ calculated with Bonn-A, MT13, and AV18 considering $R = 3$ fm in the neutron-core potential. Other values of R equals to 2, 2.5, and 3.5 fm were also used together with Bonn-A potential. We also present the values estimated with the extracted matter radius from the experimental data considering ^{11}Li as a two-neutron halo nucleus for $(\langle ^{11}\text{Li} | r_n^2 | ^{11}\text{Li} \rangle S_{2n}^{11\text{Li}})^{1/2} = 0.617(36)$ [6] and $(2/19)(\langle ^{11}\text{Li} | r_{c-2n}^2 | ^{11}\text{Li} \rangle S_{2n}^{11\text{Li}})^{1/2}$, which is in the range of 0.049 and 0.056 and denoted by “ ^{11}Li ” in the figure.

The lower panel of Fig. 6 shows the ^{19}B average angles θ_α ($\alpha \equiv nn, nc$) as a function of $-1/(a_S \kappa_{nc})$. Results are displayed for the neutron-neutron Bonn-A potential considering R with values of 2, 2.5, 3, and 3.5 fm. For MT13 and AV18 with the neutron-core potential, $R = 3$ fm. As can be seen, the angles are sensitive to the 10% difference in a_{nn} between Bonn-A and AV18 (or MT13). Interestingly, towards unitarity the relative angle between the neutrons decreases, as observed by comparing the Bonn-A and AV18 (or MT13) results. This comes from the swelling of the halo from the Borromean situation to the unitarity limit, when $1/(a_S \kappa_{nc})$ is fixed.

IV. FINAL REMARKS

We conclude from the above results that the two-neutron halo structure properties are remarkably model independent, and driven by the two-neutron separation energy and scattering lengths as long as the size of ^{17}Be is substantially smaller than the halo size. Indeed, our model confirmed that the range of the n - ^{17}Be potential $\mu^{-1} \approx 1/0.7$ fm is appreciably smaller than the halo size. The different correlations of dimensionless

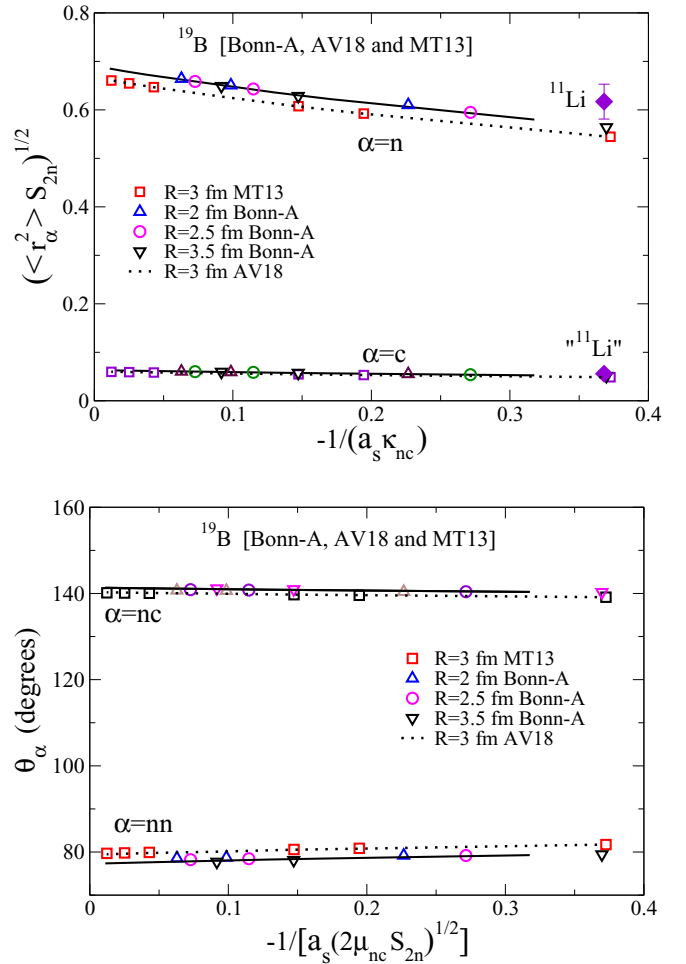


FIG. 6. Upper panel: ^{19}B dimensionless products $(\langle r_\alpha^2 \rangle S_{2n})^{1/2}$ ($\alpha \equiv n, c$) as a function of $-1/(a_S \kappa_{nc})$, where $\kappa_{nc} = (2\mu_{nc} S_{2n})^{1/2}$. Diamonds are the extracted values from experimental data on ^{11}Li . By “ ^{11}Li ” we refer to $(2/19)(\langle ^{11}\text{Li} | r_{c-2n}^2 | ^{11}\text{Li} \rangle S_{2n}^{11\text{Li}})^{1/2}$ (see text for explanation) Lower panel: average angles θ_α ($\alpha \equiv nn, nc$) as a function of $-1/(a_S \kappa_{nc})$. In both panels, symbols and lines are the same as in Fig. 5.

quantities built for the different radii, two-neutron separation energy, and scattering lengths express limit cycles governed by the Efimov-like behavior of the shallow halo ground state, and the proximity to unitarity. Notably, our numerical results for the associated scaling functions are quite independent of the radius parameter around $R \approx 3$ fm, which regulates the region where Pauli exclusion principle turns the neutron-core interaction repulsive.

Assuming that the ^{17}B core satisfies the condition of being considerably smaller than the neutron halo, we have, actually, two quantities that are not well known: the two-neutron separation energy in ^{19}B and the $n - ^{17}\text{Be}$ scattering length (in the hypothesis that one can disregard the spin-spin interaction leading to the independence on the spin states $S = 1$ and $S = 2$).

We should remark that, in the situation where the spin-spin interaction would be relevant, in the limit of large scattering

lengths the scaling functions we have addressed will have now the dependence on $a_S\kappa_{nc}$ with $S = 1^-$ and 2^- . In the unitary limit the results will be unchanged as $a_1 = a_2 \rightarrow \pm\infty$. The authors of Ref. [23] investigated the effect of wide variations of a_1 in the results obtained for S_{2n} with fixed $a_2 = -150$ fm, and it was shown that it is quite small for $-150 \lesssim a_1 \lesssim -50$ fm. Therefore, these calculations suggest that our results are quite robust even for somewhat wide difference between a_2 and a_1 provided we remain close to the unitarity limit.

Considering the recent data for the ^{19}B radius extracted from the collision experiment presented in Ref. [29] for $(\langle r_{c-2n}^2 \rangle)^{\frac{1}{2}}$ given in (1) and assuming the bounds of

$$0 < -1/[a_S(2\mu_{nc}S_{2n})^{\frac{1}{2}}] \lesssim 0.4,$$

which gives the range

$$0.5 \lesssim (\langle r_\alpha^2 \rangle S_{2n})^{\frac{1}{2}} \lesssim 0.6,$$

leading to the estimation $0.3 \lesssim S_{2n} \lesssim 0.45$ MeV. If one takes into account the scaling function for AV18 fitted as

$$(\langle r_{c-2n}^2 \rangle S_{2n})^{\frac{1}{2}} = 0.5738 + \frac{0.4191}{a_S\kappa_{nc}} + \frac{0.3188}{(a_S\kappa_{nc})^2} + \dots, \quad (14)$$

one finds $S_{2n} \simeq 0.384 \pm 0.036$ MeV obtained from the extracted value [29] of $(\langle r_{c-2n}^2 \rangle)^{\frac{1}{2}}$ given in (1) and $a_S = -150$ fm with a 50% error, consistent with the experimental upper bound [20]. Note that this value of S_{2n} is well within the estimation given above and the experimental range [21,22].

The parametrizations of the scaling functions in the upper panel of Fig. 6 are given by

$$(\langle r_n^2 \rangle S_{2n})^{\frac{1}{2}} = 0.6655 + \frac{0.4426}{a_S\kappa_{nc}} + \frac{0.3175}{(a_S\kappa_{nc})^2} + \dots \quad (15)$$

and

$$(\langle r_c^2 \rangle S_{2n})^{\frac{1}{2}} = 0.06039 + \frac{0.04440}{a_S\kappa_{nc}} + \frac{0.03418}{(a_S\kappa_{nc})^2} + \dots, \quad (16)$$

in units such that $\hbar = m_n = 1$.

The ^{17}B proton and matter radii were extracted in [47] from the experimental charge-changing cross sections of secondary beams obtained in the FRS, GSI, and Darmstadt facilities. The results from Table I in that reference are $r_p^{\text{ex}} = 2.67(2)$ fm, $r_p^{\text{ex, scaled}} = 2.63(7)$ fm, and $r_m^{\text{ex}} = 3.00(6)$, respectively. This allows us to obtain both the proton and matter radius of ^{19}B , by taking into account the previous estimations for S_{2n} and a_S introduced in the fit functions of $(\langle r_n^2 \rangle)^{\frac{1}{2}}$, Eq. (15), and $(\langle r_c^2 \rangle)^{\frac{1}{2}}$, Eq. (16), together with

$$r_m^{19\text{B}} = \sqrt{\frac{17}{19}[r_m^{\text{ex}}]^2 + \frac{2}{19}\langle r_n^2 \rangle} \quad \text{and} \quad r_p^{19\text{B}} = \sqrt{[r_p^{\text{ex}}]^2 + \langle r_c^2 \rangle},$$

which gives

$$\begin{aligned} r_m^{19\text{B}} &= 3.57 \pm 0.08 \text{ fm}, \quad r_p^{19\text{B}} = 2.74 \pm 0.02 \text{ fm for } (r_p^{\text{ex}}), \\ r_p^{19\text{B}} &= 2.70 \pm 0.07 \text{ fm for } (r_p^{\text{ex, scaled}}). \end{aligned} \quad (17)$$

Finally, in Fig. 7 we just illustrate a geometrical representation of the ^{19}B nucleus, taking for distance the scaled

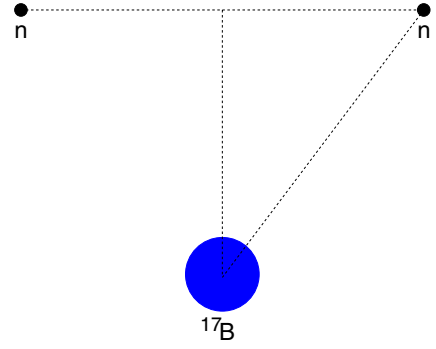


FIG. 7. Geometry of ^{19}B according to the scaled rms radii of Fig. 5. Results correspond to AV18 and to the inverse scaled scattering length $[1/a_S\kappa_{nc}] = -0.1325$.

rms radii of Fig. 5 at the inverse scaled scattering length $1/(a_S\kappa_{nc}) = -0.1325$, quoted as the experimentally extracted value [29], and using our estimated two-neutron separation energy of 0.384 MeV results in $a_S = -57$ fm, close to the lower bound of our suggested range of values for $a_S = -150 \pm 75$ fm. The geometric picture gives for the angle with vertex centered at the ^{17}B nucleus a value of 37° , close to our calculation of $\theta_{nn}/2 \simeq 40^\circ$. Furthermore from Fig. 5, we have at $1/(a_S\kappa_{nc}) = -0.1325$ the values $(\langle r_{nn}^2 \rangle S_{2n})^{\frac{1}{2}} = 0.789$, $(\langle r_{nc}^2 \rangle S_{2n})^{\frac{1}{2}} = 0.654$ and $(\langle r_{c-2n}^2 \rangle S_{2n})^{\frac{1}{2}} = 0.524$, resulting in the values of the rms relative separation distance between the neutrons, the neutron-core, and core-2n, respectively, of $\langle r_{nn}^2 \rangle^{\frac{1}{2}} = 8.2$ fm, $\langle r_{nc}^2 \rangle^{\frac{1}{2}} = 6.8$ fm, and $\langle r_{c-2n}^2 \rangle^{\frac{1}{2}} = 5.4$ fm. The latter is within the error of the extracted value [29], as written in Eq. (1). The matter and proton radius become $r_m^{19\text{B}} = 3.5$ fm and $r_p^{19\text{B}} = 2.7$ fm. These values can be compared to the estimations given in (17).

The difference between our estimations reflects the disagreement between the results from Ref. [29] and our calculations shown in Fig. 5, that does not allow us to narrow the knowledge on both the two-neutron separation energy and the $^{17}\text{B} + n$ scattering length, which calls for further experimental data and analysis. Despite that, our study of the universal properties of the two-neutron halo of ^{19}B endorses the presence of a long-range s -wave correlation between the two neutrons, as well as among the neutron and the core, exceeding by far the ranges of the nn and n -core interactions, which gives further support to the model independence of the present findings.

ACKNOWLEDGMENTS

The authors thank Valérie Lapoux for helpful discussions on the experimental charge and matter radii of ^{17}B and ^{19}B . We were granted access to the HPC resources of TGCC/IDRIS under the allocation A0110506006 made by GENCI (Grand Equipement National de Calcul Intensif). This work was supported by French IN2P3 for a theory project ‘‘Neutron-rich light unstable nuclei,’’ by the Japanese Grant-in-Aid for Scientific Research on Innovative Areas (No. 18H05407), by the CAPES/COFECUB Grant No.

88887.370819/2019-00, CNPq Grant No. 308486/2015-3, INCT-FNA Project No. 464898/2014-5, and FAPESP Thematic Grants No. 2017/05660-0 and No. 2019/07767-1. This research, initiated during the program Living Near Unitarity

at the Kavli Institute for Theoretical Physics (KITP), University of Santa Barbara (California), was supported in part by the National Science Foundation under Grant No. NSF PHY-1748958.

-
- [1] E. Nielsen, D. Fedorov, A. Jensen, and E. Garrido, *Phys. Rep.* **347**, 373 (2001).
- [2] I. Tanihata, H. Hamagaki, O. Hashimoto, Y. Shida, N. Yoshikawa, K. Sugimoto, O. Yamakawa, T. Kobayashi, and N. Takahashi, *Phys. Rev. Lett.* **55**, 2676 (1985).
- [3] A. S. Jensen, K. Riisager, D. V. Fedorov, and E. Garrido, *Rev. Mod. Phys.* **76**, 215 (2004).
- [4] E. Braaten and H. W. Hammer, *Phys. Rep.* **428**, 259 (2006).
- [5] J. Meng, H. Toki, S. G. Zhou, S. Q. Zhang, W. H. Long, and L. S. Geng, *Prog. Part. Nucl. Phys.* **57**, 470 (2006).
- [6] T. Frederico, A. Delfino, L. Tomio, and M. T. Yamashita, *Prog. Part. Nucl. Phys.* **67**, 939 (2012).
- [7] I. Tanihata, H. Savajols, and R. Kanungo, *Prog. Part. Nucl. Phys.* **68**, 215 (2013).
- [8] K. Riisager, *Phys. Scr.* **2013**, 014001.
- [9] N. T. Zinner and A. S. Jensen, *J. Phys. G: Nucl. Part. Phys.* **40**, 053101 (2013).
- [10] L. F. Canto, P. R. S. Gomes, R. Donangelo, J. Lubian, and M. S. Hussein, *Phys. Rep.* **596**, 1 (2015).
- [11] P. Naidon and S. Endo, *Rep. Prog. Phys.* **80**, 056001 (2017).
- [12] H. W. Hammer, C. Ji, and D. R. Phillips, *J. Phys. G: Nucl. Part. Phys.* **44**, 103002 (2017).
- [13] C. H. Greene, P. Giannakeas, and J. Perez-Rios, *Rev. Mod. Phys.* **89**, 035006 (2017).
- [14] H. W. Hammer, [arXiv:2203.13074](https://arxiv.org/abs/2203.13074) [nucl-th].
- [15] I. Mazumdar, V. Arora, and V. S. Bhasin, *Phys. Rev. C* **61**, 051303(R) (2000).
- [16] M. T. Yamashita, R. S. M. de Carvalho, T. Frederico, and L. Tomio, *Phys. Lett. B* **697**, 90 (2011); **715**, 282(E) (2012).
- [17] B. Acharya, C. Ji, and D. R. Phillips, *Phys. Lett. B* **723**, 196 (2013).
- [18] K. Tanaka, T. Yamaguchi, T. Suzuki, T. Ohtsubo, M. Fukuda, D. Nishimura, M. Takechi, K. Ogata, A. Ozawa, and T. Izumikawa *et al.*, *Phys. Rev. Lett.* **104**, 062701 (2010).
- [19] Y. Togano, T. Nakamura, Y. Kondo, J. A. Tostevin, A. T. Saito, J. Gibelin, N. A. Orr, N. L. Achouri, T. Aumann and H. Baba *et al.*, *Phys. Lett. B* **761**, 412 (2016).
- [20] A. Spyrou *et al.*, *Phys. Lett. B* **683**, 129 (2010).
- [21] L. Gaudefroy *et al.*, *Phys. Rev. Lett.* **109**, 202503 (2012).
- [22] M. Wang, G. Audi, F. G. Kondev, W. Huang, S. Naimi, and X. Xu, *Chin. Phys. C* **41**, 030003 (2017).
- [23] E. Hiyama, R. Lazauskas, F. Miguel Marqués, J. Carbonell, *Phys. Rev. C* **100**, 011603(R) (2019).
- [24] V. Efimov, *Phys. Lett. B* **33**, 563 (1970).
- [25] V. N. Efimov, *Sov. J. Nucl. Phys.* **12**, 589 (1971).
- [26] A. E. A. Amorim, T. Frederico, and L. Tomio, *Phys. Rev. C* **56**, R2378(R) (1997).
- [27] D. L. Canham and H. W. Hammer, *Eur. Phys. J. A* **37**, 367 (2008).
- [28] V. Efimov, *Comments Nucl. Part. Phys.* **19**, 271 (1990).
- [29] K. J. Cook *et al.*, *Phys. Rev. Lett.* **124**, 212503 (2020).
- [30] J. Casal and E. Garrido, *Phys. Rev. C* **102**, 051304(R) (2020).
- [31] X. X. Sun, *Phys. Rev. C* **103**, 054315 (2021).
- [32] M. T. Yamashita, L. Tomio, and T. Frederico, *Nucl. Phys. A* **735**, 40 (2004).
- [33] T. Suzuki *et al.*, *Nucl. Phys. A* **658**, 313 (1999).
- [34] R. Machleidt, K. Holinde, Ch. Elster, *Phys. Rep.* **149**, 1 (1987).
- [35] R. B. Wiringa, V. G. J. Stoks, and R. Schiavilla, *Phys. Rev. C* **51**, 38 (1995).
- [36] R. A. Malfliet and J. A. Tjon, *Nucl. Phys. A* **127**, 161 (1969).
- [37] E. Hiyama, Y. Kino, and M. Kamimura, *Prog. Part. Nucl. Phys.* **51**, 223 (2003).
- [38] R. Lazauskas and J. Carbonell, *Phys. Rev. C* **71**, 044004 (2005).
- [39] R. Lazauskas and J. Carbonell, *Phys. Rev. C* **72**, 034003 (2005).
- [40] L. Madeira, T. Frederico, S. Gandolfi, L. Tomio, and M. T. Yamashita, *Phys. Rev. A* **104**, 033301 (2021).
- [41] S. Tan, *Ann. Phys.* **323**, 2952 (2008).
- [42] A. E. A. Amorim, L. Tomio, and T. Frederico, *Phys. Rev. C* **46**, 2224 (1992).
- [43] Y. Castin and F. Werner, *Phys. Rev. A* **83**, 063614 (2011).
- [44] D. Gogny, P. Pires, and R. D. Tournel, *Phys. Lett. B* **32**, 591 (1970).
- [45] T. Nakamura, A. M. Vinodkumar, T. Sugimoto, N. Aoi, H. Baba, D. Bazin, N. Fukuda, T. Gomi, H. Hasegawa, N. Imai, *et al.*, *Phys. Rev. Lett.* **96**, 252502 (2006).
- [46] M. Smith *et al.*, *Phys. Rev. Lett.* **101**, 202501 (2008).
- [47] A. Estradé, R. Kanungo, W. Horiuchi, F. Ameil, J. Atkinson, Y. Ayyad, D. Cortina-Gil, I. Dillmann, A. Evdokimov, and F. Farinon *et al.*, *Phys. Rev. Lett.* **113**, 132501 (2014).